DOI: 10.1002/cmdc.200500015

Aroyl-Pyrrolyl Hydroxyamides: Influence of Pyrrole C4-Phenylacetyl Substitution on Histone Deacetylase Inhibition**

Antonello Mai,*[a] Silvio Massa,[c] Sergio Valente,[a] Silvia Simeoni,[a] Rino Ragno,[a] Patrizia Bottoni,[d] Roberto Scatena,[d] and Gerald Brosch*[b]

*The novel aroyl-pyrrolyl hydroxyamides **4a**–**a**′ are analogues of the lead compound 3-(1-methyl-4-phenylacetyl-1H-pyrrol-2-yl)-N-hydroxy-2-propenamide (**2**) and are active as HDAC inhibitors. The benzene ring of **2** was substituted with a wide range of electron-donating and electron-withdrawing groups, and the effect was evaluated on three HDACs from maize, namely HD2, HD1-B (a class I HDAC), and HD1-A (a class II HDAC). Inhibition studies show that the benzene 3′ and, to a lesser extent, 4′ positions of **2** were the most suitable for the introduction of substituents, with the 3′-chloro (in **4b**) and the 3′-methyl (in **4k**) derivatives being the most potent compounds, reaching the same activity as SAHA. Inhibition data for **4b**,**k** against mouse HDAC1 were consistent with those observed in the maize enzyme. The substituent insertion on the benzene ring of **2** (compounds **4a**–**a**′) abated the slight (3-fold) selectivity for class II HDACs displayed by **2**. Compound **4b** showed interesting, dose-dependent antiproliferative and cytodifferentiation properties against human acute promyelocytic leukemia HL-60 cells.*

Introduction

The reversible modification of nuclear histones by acetylation is controlled and maintained by the activities of two families of enzymes: histone acetyltransferases (HATs) and histone deacetylases (HDACs). Such modifications play a crucial role in gene expression.[1–7] Hypoacetylated histones lead to transcriptional repression by condensing the structure of chromatin and restricting the access of transcription factors. Conversely, histone acetylation has been associated with relaxed chromatin structure and active gene transcription.[8–11] Aberrant regulation of this epigenetic mechanism has been shown to cause inappropriate gene expression, a key event in the pathogenesis of many forms of cancer.[12–15] Moreover, HDAC inhibition elicits growth arrest, differentiation, and/or apoptosis in many types of tumor cells by reactivating the transcription of a small number of genes.[16–24]

Currently, mammalian HDACs are separated into three classes according to their homology with enzymes initially identified in yeast. Yeast RPD3, HDA1, and Sir2 are the founding members of class I, II, and III HDACs, respectively.[24,25] Another eukaryotic deacetylase, maize HD2, is structurally quite different from mammalian HDACs and has been assigned to a class of its own.[26] Class I and II enzymes use a Zn^{+2}-dependent mechanism of deacetylation, are found in multiprotein complexes targeted to specific chromatin domains, and are inhibited by natural (trichostatin A, TSA) or synthetic (suberoylanilide hydroxamic acid, SAHA) HDAC inhibitors (Figure 1).[24,25] Class III HDACs are insensitive to class I/II HDAC inhibitors. Equipped with the NAD^{+} coenzyme, they catalyze the transfer of the acetyl group of an acetyllysine residue to the nicotinamide-deprived ADP-ribose group.[27]

Class I HDACs are well-known transcriptional co-repressors, which act by blocking the expression of some tumor-suppressor genes.[16,24] Class II HDACs have been reported to interact with one or more DNA-binding transcription factors, as well as with transcriptional co-repressors such as MEF2.[28] The development of new molecules that are able to selectively inhibit only a (sub)class of the HDAC family is a very attractive goal to

[a] *Prof. A. Mai, Dr. S. Valente, Dr. S. Simeoni, Dr. R. Ragno*
Istituto Pasteur—Fondazione Cenci Bolognetti
Dipartimento di Studi Farmaceutici
Università degli Studi di Roma "La Sapienza"
P.le A. Moro 5, 00185 Roma (Italy)
Fax: (+390) 396-491491
E-mail: antonello.mai@uniroma1.it

[b] *Prof. G. Brosch*
Department of Molecular Biology
Innsbruck Medical University
Peter-Mayr-Strasse 4b, 6020 Innsbruck (Austria)
Fax: (+43) 512-507-2866
E-mail: gerald.brosch@uibk.ac.at

[c] *Prof. S. Massa*
Dipartimento Farmaco Chimico Tecnologico
Università degli Studi di Siena
via A. Moro, 53100 Siena (Italy)

[d] *Dr. P. Bottoni, Prof. R. Scatena*
Istituto di Biochimica e Biochimica Clinica
Università Cattolica del Sacro Cuore
L.go F. Vito 1, 00168 Roma (Italy)

[**] *Previous papers in this series: A. Mai, S. Massa, I. Cerbara, S. Valente, R. Ragno, P. Bottoni, R. Scatena, P. Loidl, G. Brosch,* J. Med. Chem. ***2004***, 47, *1098–1109.*

Supporting information for this article is available on the WWW under http://www.chemmedchem.org or from the author.

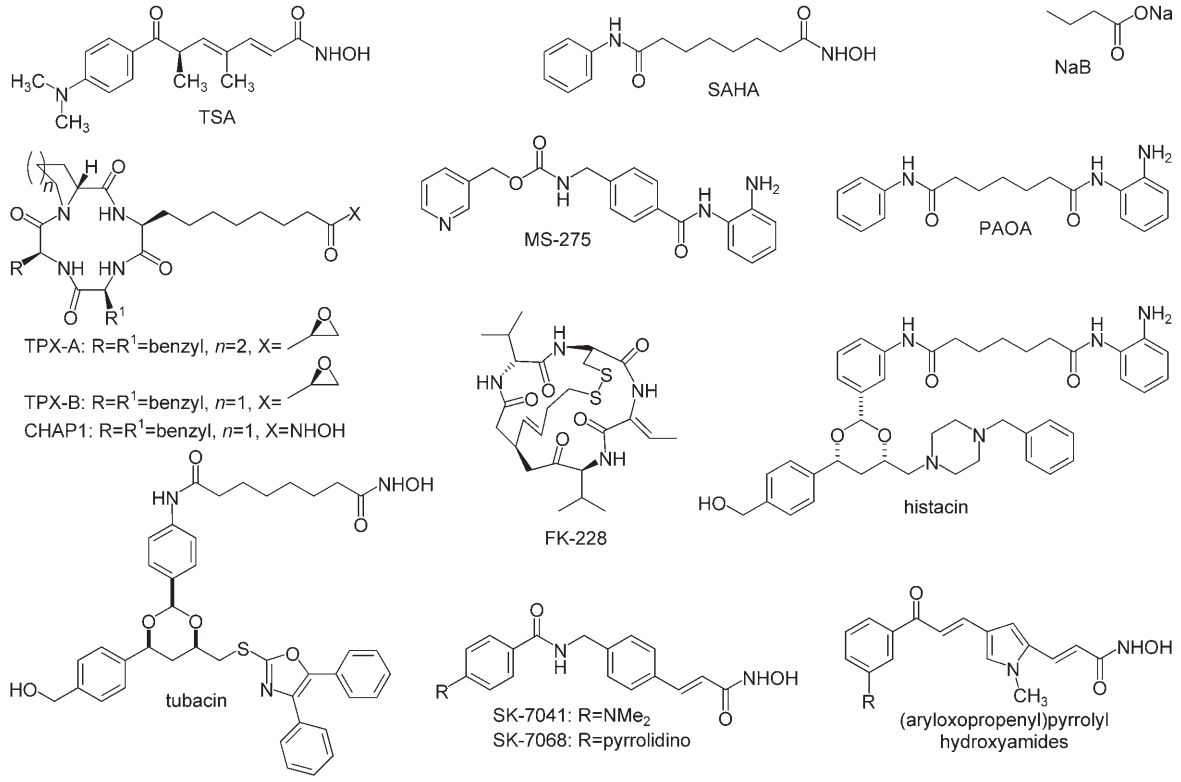

Figure 1. Structures of known HDAC inhibitors.

pursue, because such compounds could be useful tools to distinguish the unique functions of the different HDACs, and could represent highly specific cancer therapies with greatly decreased toxicity.

A large number of natural and synthetic class I/II HDAC inhibitors have been reported so far, and the majority of them do not discriminate between the different classes of enzymes.[17–24] The only exceptions are sodium valproate (VPA),[29] some 2′-aminoanilides (such as MS-275,[30,31] histacin,[32] and pimeloyl-anilide orthoaminoanilide (PAOA)[32]), a few cinnamyl hydroxamates (SK-7041 and SK-7068),[33] and depsipeptide FK-228,[34] which are class I-selective HDAC inhibitors. Trapoxins (TPXs), cyclic hydroxamic acid-containing peptide 1 (CHAP1), and sodium butyrate (NaB) are ineffective in inhibiting HDAC6,[35,36] whereas tubacin[37–39] and some aryloxopropenyl-pyrrolyl hydroxyamides[40] are class IIb- and class II (IIa)-selective HDAC inhibitors, respectively (Figure 1).

According to these findings, we undertook synthetic and biological efforts to improve the HDAC inhibitory activity of the aroyl-pyrrolyl hydroxyamides (APHAs) recently reported by us (Figure 2).[41–45] Starting from the first lead compound, 3-(4-benzoyl-1-methyl-1*H*-pyrrol-2-yl)-*N*-hydroxy-2-propenamide (**1**) (Figure 3),[41,42] we performed some chemical modifications on the structure of **1** to increase its anti-HDAC activity. Among the modifications described, only the insertion of a phenylacetyl/phenylpropionyl moiety at the C4 position of the pyrrole ring led to an improved anti-HDAC potency of the inhibitors, affording compounds **2** and **3** (Figure 3).[43,44] Furthermore, **2** and **3** were tested against maize HD1-B[46,47] and HD1-A,[48,49] two mammalian class I and class II HDAC homologues, to explore their potential class-selectivity. In these tests, **2** and **3** showed similar activities (**2**: $IC_{50(HD1\text{-}B)} = 150$ nM, $IC_{50(HD1\text{-}A)} = 50$ nM; **3**: $IC_{50(HD1\text{-}B)} = 120$ nM, $IC_{50(HD1\text{-}A)} =$

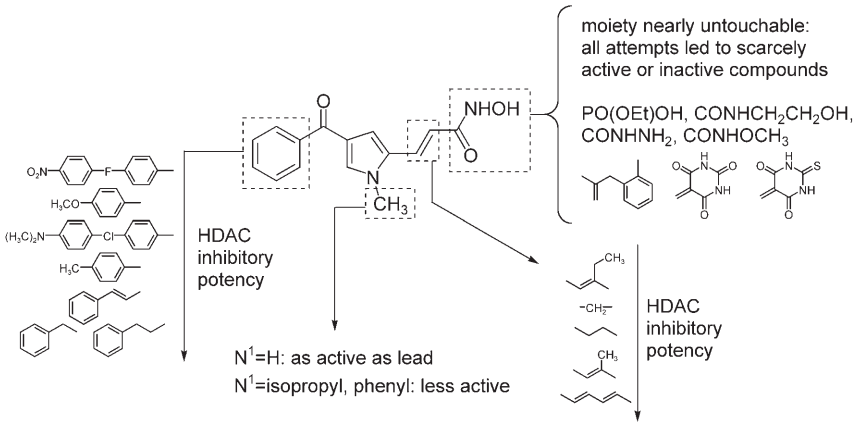

Figure 2. Structure–activity relationship (SAR) summary of aroyl-pyrrolyl hydroxyamides (APHAs).

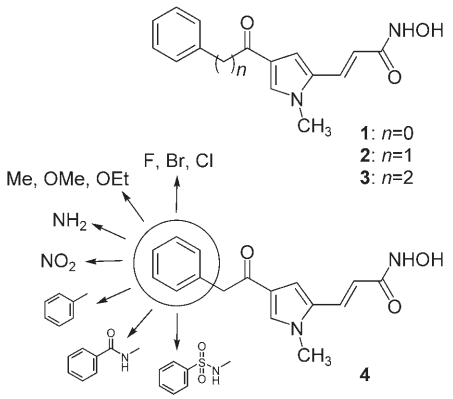

Figure 3. APHA lead compounds and new designed derivatives.

60 nM), with **2** having higher selectivity for class II than **3** (selectivity for class II HDACs: **2**, 3-fold; **3**, 2-fold). Compounds **2** and **3** showed similar antiproliferative and cytodifferentiation properties in assays with Friends murine erythroleukemia (MEL) cells.[44]

As **2** and **3** showed similar behaviors both in vitro and in vivo, we chose the phenylacetyl-pyrrolyl hydroxypropenamide template of **2** for chemical investigation. In particular, we introduced various substituents ranging between electron-donating and electron-withdrawing groups, in the *ortho*, *meta*, or *para* positions of the benzene ring (compounds **4**, Figure 3). The influence of such insertions on the inhibitory activities toward HD2 as well as HD1-B and HD1-A was evaluated, and the potential class-selectivity of the novel derivatives was assessed.

Selected title compounds **4b**,**k** were tested against mouse HDAC1 in comparison with **2** and SAHA. Homology models, molecular modeling, and docking studies were performed on the most selective derivatives against HD1-B (compound **4u**) and HD1-A (compound **4t**), to gain insight about their binding mode. Finally, the most potent compound, **4b**, was evaluated as an antiproliferative and cytodifferentiation agent in human acute promyelocytic leukemia HL-60 cells.

Chemistry

Ethyl 3-[1-methyl-4-(substituted)phenylacetyl-1*H*-pyrrol-2-yl]-2-propenoates **7a**–**w**, key intermediates for the synthesis of the hydroxamates **4**, were prepared by the one-pot Vilsmeier–Haack/Friedel–Crafts reaction performed on 1-methyl-1*H*-pyrrole with oxalyl chloride/*N*,*N*-dimethylformamide and (substituted)phenylacetyl chloride/aluminum trichloride, followed by Wittig–Horner reaction of the obtained aroyl-pyrrolecarboxaldehydes **6a**–**w** with triethylphosphonoacetate and potassium carbonate (Scheme 1a). 3-Ethoxyphenylacetic acid, useful for the synthesis of the pyrrolealdehyde **6r**, was prepared as reported.[50] A Suzuki coupling reaction between methyl 3-bromophenylacetate and phenylboronic acid in the presence of tetrakis(triphenylphosphine)palladium and sodium carbonate followed by alkaline hydrolysis afforded, with a simple two-step method, the 3-biphenylacetic acid **5a**,[51] which was used

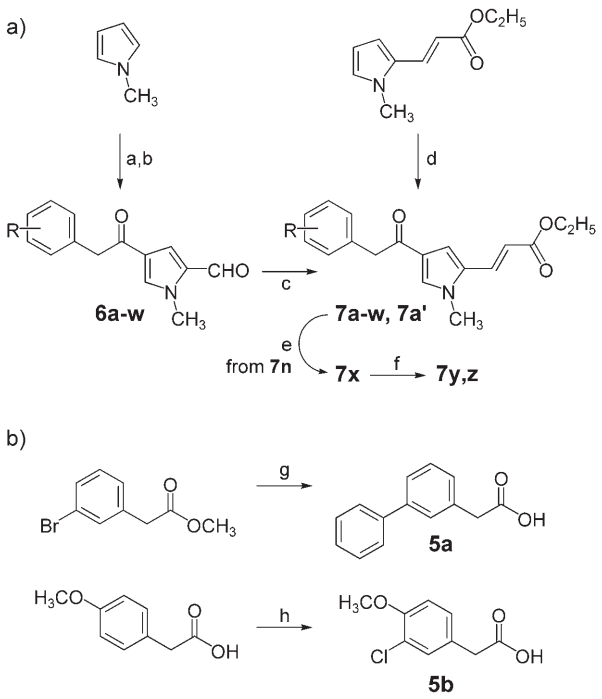

Scheme 1. a) Oxalyl chloride, DMF, RT; b) 1. R-Ph-CH_2COCl, $AlCl_3$, 1,2-dichloroethane, RT, 2. KOH, H_2O, RT; c) $(C_2H_5O)_2OPCH_2COOC_2H_5$, K_2CO_3, C_2H_5OH, 80 °C; d) **5b**, $SOCl_2$, $AlCl_3$, 1,2-dichloroethane, RT; e) $NaHPO_2$, K_2CO_3, Pd/C, THF/H_2O, RT; f) benzoyl chloride or benzenesulfonyl chloride, $(C_2H_5)_3N$, dichloromethane, RT; g) 1. phenylboronic acid, Na_2CO_3, tetrakis(triphenylphosphine)palladium, Ph-CH_3/C_2H_5OH, 80 °C, 2. KOH, H_2O, RT; h) potassium peroxymonosulfate (oxone), NaCl, acetone/H_2O, RT.

for the synthesis of **6t** (Scheme 1b). A single-step, high-yielding reaction of 4-methoxyphenylacetic acid with potassium peroxymonosulfate (oxone) and sodium chloride led to the 3-chloro-4-methoxyphenylacetic acid **5b**[52] (Scheme 1b), which was useful in the preparation of the ethyl 3-[4-(3-chloro-4-methoxyphenylacetyl)-1-methyl-1*H*-pyrrol-2-yl]-2-propenoate **7a′**. Such compounds, the preparation of which failed with the Vilsmeier–Haack/Friedel–Crafts procedure, was obtained by acylation of ethyl (1-methyl-1*H*-pyrrol-2-yl)-2-propenoate[53] with aluminum trichloride and 3-chloro-4-methoxyphenylacetyl chloride (Scheme 1a).

Ethyl 3-[4-(3-benzoylamino- and 3-benzenesulfonylaminophenylacetyl)-1-methyl-1*H*-pyrrol-2-yl]-2-propenoates **7y**,**z** were prepared by the reaction of benzoyl chloride or benzenesulfonyl chloride with ethyl 3-[4-(3-aminophenylacetyl)-1-methyl-1*H*-pyrrol-2-yl]-2-propenoate **7x**, previously obtained by reduction of the 3-nitro analogue **7n** with sodium hypophosphite and potassium carbonate (Scheme 1a). Alkaline hydrolysis of the ethyl pyrrole-propenoates **7a**–**a′** furnished the pyrrole-propenoic acids **8a**–**a′**, which were in turn converted into the corresponding hydroxamates **4a**–**a′** through reaction with ethyl chloroformate and *O*-(2-methoxy-2-propyl)hydroxylamine,[54] followed by acid hydrolysis of the *N*-(1-methoxy-1-methylethoxy)propenamides **9a**–**a′** with the Amberlyst 15 ion-exchange resin (Scheme 2). The *O*-protected hydroxamates **9** were hydrolyzed without further purification as soon as they were obtained.

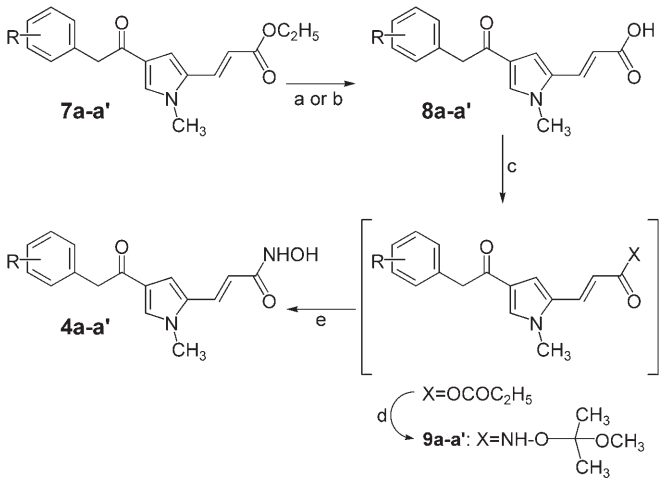

Scheme 2. a) KOH, C_2H_5OH, H_2O, 70 °C; b) LiOH, H_2O, RT; c) $ClCOOC_2H_5$, $(C_2H_5)_3N$, THF, 0 °C; d) $NH_2OC(CH_3)_2OCH_3$, RT; e) Amberlyst 15, CH_3OH, RT.

Chemical and physical data for compounds **4a**–**a**′ are listed in Table 1. Chemical and physical data for the intermediate compounds **5**–**8** are listed in Table 2.

Results and Discussion

The novel APHA compounds **4a**–**a**′ (Figure 3) were evaluated for their ability to inhibit maize HDACs. The maize system offers the advantage that three different types of HDACs can be biochemically separated: class I (HD1-B)[46,47] and class II (HD1-A)[48,49] enzymes, and the plant-specific form HD2.[26,55–58]

Two short-chain fatty acids (NaB[59] and VPA[29,60]), two hydroxamic acids (TSA[61] and SAHA[62]), two cyclic tetrapeptides (TPX[63] and HC-toxin[64]), PAOA (a class I-selective inhibitor),[32] and tubacin (an in-cell class IIb-selective inhibitor[32,37–39]) have been reported as reference drugs in anti-HD2 assays. The results, expressed as the percent inhibition at a fixed dose and IC_{50} (50% inhibitory concentration) values, are reported in Table 3. In assays for HD1-B and HD1-A inhibition, TSA, SAHA, PAOA, tubacin, **2**, and **3** were also tested for the purpose of comparison (Table 4). Selected compounds (3′-chloro (compound **4b**) and 3′-methyl (compound **4k**) derivatives) were tested against mouse HDAC1 in comparison with **2** and SAHA (Table 5).

Anti-HD2 activity and structure–activity relationships (SARs)

In the anti-HD2 assay, 3′-chloro- (compound **4b**), 3′-fluoro- (compound **4e**), 3′-bromo- (compound **4h**), and 3′-methyl-substituted (compound **4k**) pyrroles showed higher anti-HD2 activity than **2**. With the insertion of a nitro group (regardless of its position on the benzene ring) only weak inhibitors **4m**–**o** were obtained. Conversely, the introduction of a methoxy (but not an ethoxy!) group at either the 3′ or 4′ position of the benzene ring led to compounds **4p**,**q** more potent than **2**, whereas the bulky phenyl substituent was well-tolerated at the *para* position (in **4u**) but not at the *meta* position (in **4t**). Reduction of the 3′-nitro group to the 3′-amino function (from **4n** to **4x**) strongly abated the inhibitory activity toward HD2, but this activity was promptly restored by replacement of the amine group (in **4x**) with an amide function (in **4y**,**z**).

Table 1. Chemical and physical data for compounds **4a**–**a**′.

Compd	R	mp [°C]	Recrystallization Solvent	Yield [%]	Formula	Anal[a]
4a	2-Cl	>250	acetonitrile	58	$C_{16}H_{15}ClN_2O_3$	C, H, N, Cl
4b	3-Cl	162–163	benzene/acetonitrile	52	$C_{16}H_{15}ClN_2O_3$	C, H, N, Cl
4c	4-Cl	175–177	acetonitrile	66	$C_{16}H_{15}ClN_2O_3$	C, H, N, Cl
4d	2-F	188–190	benzene/acetonitrile	54	$C_{16}H_{15}FN_2O_3$	C, H, N, F
4e	3-F	199-201	acetonitrile/benzene	57	$C_{16}H_{15}FN_2O_3$	C, H, N, F
4f	4-F	178–179	benzene/acetonitrile	68	$C_{16}H_{15}FN_2O_3$	C, H, N, F
4g	2-Br	180–182	benzene/acetonitrile	49	$C_{16}H_{15}BrN_2O_3$	C, H, N, Br
4h	3-Br	163–165	benzene/acetonitrile	55	$C_{16}H_{15}BrN_2O_3$	C, H, N, Br
4i	4-Br	153–154	benzene/acetonitrile	64	$C_{16}H_{15}BrN_2O_3$	C, H, N, Br
4j	2-Me	>250	acetonitrile	52	$C_{17}H_{18}N_2O_3$	C, H, N
4k	3-Me	210–212	acetonitrile/benzene	57	$C_{17}H_{18}N_2O_3$	C, H, N
4l	4-Me	>250	acetonitrile	54	$C_{17}H_{18}N_2O_3$	C, H, N
4m	2-NO_2	180–182	benzene/acetonitrile	45	$C_{16}H_{15}N_3O_5$	C, H, N
4n	3-NO_2	228–230	acetonitrile	58	$C_{16}H_{15}N_3O_5$	C, H, N
4o	4-NO_2	118–120	benzene/acetonitrile	59	$C_{16}H_{15}N_3O_5$	C, H, N
4p	3-OMe	148–150	benzene/acetonitrile	43	$C_{17}H_{18}N_2O_4$	C, H, N
4q	4-OMe	178–180	benzene/acetonitrile	56	$C_{17}H_{18}N_2O_4$	C, H, N
4r	3-OEt	100–102	benzene	48	$C_{18}H_{20}N_2O_4$	C, H, N
4s	4-OEt	190–192	benzene/acetonitrile	44	$C_{18}H_{20}N_2O_4$	C, H, N
4t	3-Ph	117–118	benzene	42	$C_{22}H_{20}N_2O_3$	C, H, N
4u	4-Ph	199–201	benzene/acetonitrile	58	$C_{22}H_{20}N_2O_3$	C, H, N
4v	3,5-Me_2	194–196	acetonitrile/ethanol	58	$C_{18}H_{20}N_2O_3$	C, H, N
4w	3,5-F_2	143–145	benzene/acetonitrile	56	$C_{16}H_{14}F_2N_2O_3$	C, H, N, F
4x	3-NH_2	201–202	benzene/acetonitrile	53	$C_{16}H_{17}N_3O_3$	C, H, N
4y	3-NHCOPh	222–225	benzene/acetonitrile	40	$C_{23}H_{21}N_3O_4$	C, H, N
4z	3-$NHSO_2$Ph	75–77	diethyl ether	42	$C_{22}H_{20}N_3O_5S$	C, H, N, S
4a′	3-Cl-4-OMe	100–102	diethyl ether	55	$C_{17}H_{17}ClN_2O_4$	C, H, N, Cl

[a] Analytical results were within ±0.4% of theoretical values.

HD1-B and HD1-A inhibitory effects: class-selectivity assessment

In assays against the maize class I (HD1-B) and class II (HD1-A) HDACs, 3-[1-methyl-4-phenylacetyl- and 3-[1-methyl-4-(3-phenylpropionyl)-1*H*-pyrrol-2-yl]-*N*-hydroxy-2-propenamides **2** and **3** showed inhibitory activity in the sub-micromolar range; both are more potent against HD1-A than HD1-B (selectivity for class II: **2**, 3-fold; **3**, 2-fold; Table 4). To explore the effect of substituent insertion on class selectivity, we assayed **4a**–**a**′ against HD1-B

Table 2. Chemical and physical data for compounds **5**–**8**.

Compd	R	mp [°C]	Recrystallization Solvent	Yield [%]	Formula	Anal[a]
5a		141–143	benzene/cyclohexane	84	$C_{14}H_{12}O_2$	C, H
5b		98–100	benzene/cyclohexane	90	$C_9H_9ClO_3$	C, H, Cl
6a	2-Cl	101–102	benzene/cyclohexane	56	$C_{14}H_{12}ClNO_2$	C, H, N, Cl
6b	3-Cl	86–88	diethyl ether	41	$C_{14}H_{12}ClNO_2$	C, H, N, Cl
6c	4-Cl	110–111	benzene	57	$C_{14}H_{12}ClNO_2$	C, H, N, Cl
6d	2-F	89–91	cyclohexane/benzene	65	$C_{14}H_{12}FNO_2$	C, H, N, F
6e	3-F	48–50	diethyl ether	70	$C_{14}H_{12}FNO_2$	C, H, N, F
6f	4-F	85–87	benzene/cyclohexane	83	$C_{14}H_{12}FNO_2$	C, H, N, F
6g	2-Br	94–95	benzene/cyclohexane	54	$C_{14}H_{12}BrNO_2$	C, H, N, Br
6h	3-Br	104–105	benzene/cyclohexane	64	$C_{14}H_{12}BrNO_2$	C, H, N, Br
6i	4-Br	128–130	benzene/cyclohexane	72	$C_{14}H_{12}BrNO_2$	C, H, N, Br
6j	2-Me	111–112	cyclohexane	42	$C_{15}H_{15}NO_2$	C, H, N
6k	3-Me	54–55	cyclohexane	58	$C_{15}H_{15}NO_2$	C, H, N
6L	4-Me	110–111	benzene/cyclohexane	90	$C_{15}H_{15}NO_2$	C, H, N
6m	2-NO_2	134–136	benzene	38	$C_{14}H_{12}N_2O_4$	C, H, N
6n	3-NO_2	126–128	benzene/cyclohexane	87	$C_{14}H_{12}N_2O_4$	C, H, N
6o	4-NO_2	135–136	benzene/cyclohexane	76	$C_{14}H_{12}N_2O_4$	C, H, N
6p	3-OMe	88–90	benzene/cyclohexane	58	$C_{15}H_{15}NO_3$	C, H, N
6q	4-OMe	149–151	benzene/cyclohexane	66	$C_{15}H_{15}NO_3$	C, H, N
6r	3-OEt	94–95	cyclohexane	42	$C_{16}H_{17}NO_3$	C, H, N
6s	4-OEt	125–127	benzene/cyclohexane	53	$C_{16}H_{17}NO_3$	C, H, N
6t	4-Ph	78–80	diethyl ether	41	$C_{20}H_{17}NO_2$	C, H, N
6u	3,5-Me_2	oil		62	$C_{16}H_{17}NO_2$	C, H, N
6v	3,5-F_2	146–147	benzene/cyclohexane	57	$C_{14}H_{11}F_2NO_2$	C, H, N, F
7a	2-Cl	209–210	benzene/cyclohexane	42	$C_{18}H_{18}ClNO_3$	C, H, N, Cl
7b	3-Cl	oil		95	$C_{18}H_{18}ClNO_3$	C, H, N, Cl
7c	4-Cl	oil		73	$C_{18}H_{18}ClNO_3$	C, H, N, Cl
7d	2-F	95–97	benzene/cyclohexane	88	$C_{18}H_{18}FNO_3$	C, H, N, F
7e	3-F	oil		86	$C_{18}H_{18}FNO_3$	C, H, N, F
7f	4-F	93–94	benzene/cyclohexane	91	$C_{18}H_{18}FNO_3$	C, H, N, F
7g	2-Br	99–101	benzene/cyclohexane	75	$C_{18}H_{18}BrNO_3$	C, H, N, Br
7h	3-Br	111–112	benzene/cyclohexane	79	$C_{18}H_{18}BrNO_3$	C, H, N, Br
7i	4-Br	136–137	benzene/cyclohexane	89	$C_{18}H_{18}BrNO_3$	C, H, N, Br
7j	2-Me	124–126	benzene/acetonitrile	68	$C_{19}H_{21}NO_3$	C, H, N
7k	3-Me	80–82	cyclohexane	77	$C_{19}H_{21}NO_3$	C, H, N
7L	4-Me	54–56	cyclohexane	95	$C_{19}H_{21}NO_3$	C, H, N
7m	2-NO_2	94–96	diethyl ether	81	$C_{18}H_{18}N_2O_5$	C, H, N
7n	3-NO_2	128–130	benzene/cyclohexane	87	$C_{18}H_{18}N_2O_5$	C, H, N
7o	4-NO_2	129–131	benzene/cyclohexane	78	$C_{18}H_{18}N_2O_5$	C, H, N
7p	3-OMe	91–93	benzene	60	$C_{19}H_{21}NO_4$	C, H, N
7q	4-OMe	85–87	diethylester	72	$C_{19}H_{21}NO_4$	C, H, N
7r	3-OEt	99–100	benzene/cyclohexane	67	$C_{20}H_{23}NO_4$	C, H, N
7s	4-OEt	73–75	cyclohexane	63	$C_{20}H_{23}NO_4$	C, H, N
7t	3-Ph	oil		45	$C_{24}H_{23}NO_3$	C, H, N
7u	4-Ph	130–132	benzene/cyclohexane	74	$C_{24}H_{23}NO_3$	C, H, N
7v	3,5-Me_2	oil		59	$C_{20}H_{23}NO_3$	C, H, N
7w	3,5-F_2	154–156	benzene	63	$C_{18}H_{17}F_2NO_3$	C, H, N, F
7x	3-NH_2	oil		63	$C_{18}H_{20}N_2O_3$	C, H, N
7y	3-NHCOPh	oil		53	$C_{25}H_{24}N_2O_4$	C, H, N
7z	3-$NHSO_2$Ph	oil		59	$C_{24}H_{24}N_2O_5S$	C, H, N, S
7a′	3-Cl-4-OMe	104–105	benzene/cyclohexane	67	$C_{19}H_{20}ClNO_4$	C, H, N, Cl
8a	2-Cl	210–212	benzene/cyclohexane	74	$C_{16}H_{14}ClNO_3$	C, H, N, Cl
8b	3-Cl	195–196	acetonitrile	65	$C_{16}H_{14}ClNO_3$	C, H, N, Cl
8c	4-Cl	207–209	acetonitrile	74	$C_{16}H_{14}ClNO_3$	C, H, N, Cl
8d	2-F	185–187	benzene/acetonitrile	78	$C_{16}H_{14}FNO_3$	C, H, N, F
8e	3-F	105–107	benzene	67	$C_{16}H_{14}FNO_3$	C, H, N, F
8f	4-F	169–171	benzene/acetonitrile	73	$C_{16}H_{14}FNO_3$	C, H, N, F
8g	2-Br	210–211	benzene/acetonitrile	81	$C_{16}H_{14}BrNO_3$	C, H, N, Br
8h	3-Br	209–210	benzene/acetonitrile	84	$C_{16}H_{14}BrNO_3$	C, H, N, Br
8i	4-Br	178–180	benzene/acetonitrile	87	$C_{16}H_{14}BrNO_3$	C, H, N, Br
8j	2-Me	204–205	acetonitrile	75	$C_{17}H_{17}NO_3$	C, H, N
8k	3-Me	160–161	acetonitrile	79	$C_{17}H_{17}NO_3$	C, H, N
8l	4-Me	189–190	acetonitrile	77	$C_{17}H_{17}NO_3$	C, H, N
8m	2-NO_2	230–232	benzene/acetonitrile	68	$C_{16}H_{14}N_2O_5$	C, H, N
8n	3-NO_2	260–262	acetonitrile	85	$C_{16}H_{14}N_2O_5$	C, H, N

and HD1-A, in comparison with TSA, SAHA, and PAOA (class I-selective inhibitors), and tubacin (an in-cell class IIb-selective inhibitor) (Table 4).

Halogen atom and methyl group substitution at the 3′ (compounds **4b**,**e**,**h**,**k**) or 4′ position (compounds **4c**,**f**,**i**) of the pyrrole-C4 phenylacetyl moiety led to compounds with higher inhibitory activity against HD1-B than **2**. Among the 2′-substituted analogues, only the 2′-fluoro derivative **4d** was 3–4-fold more potent than **2** against HD1-B. Little or no effect of benzene substitution was observed on the inhibitory activity toward HD1-A; the 3′-halogen/methyl-substituted compounds **4b**,**e**,**h**,**k** and the 2′-fluoro analogue **4d** were 2-fold more potent than **2**.

None of the newly substituted compounds were class-selective. Among them, only the 4-nitropyrrole **4o** showed a slight selectivity for class I (2-fold). The introduction of a phenyl substituent at the 3′ position of the benzene ring (compound **4t**) decreased the anti-HD1-B and, to a lesser extent, the anti-HD1-A activities of the derivative; **4t** showed a 3.6-fold selectivity in favor of class II deacetylase. Conversely, its 4′-phenyl counterpart **4u** was very potent against both enzymes and showed a small class I selectivity ratio (2.5-fold).

The anti-HD1-B assay revealed TSA and SAHA to be endowed with strong inhibitory activity, with TSA active at sub-nanomolar concentrations (IC_{50} = 0.4 nM), and with SAHA showing an IC_{50} value of 30 nM. The 3′-chloro- (compound **4b**), 2′-fluoro- (compound **4d**), 3′-bromo- (compound **4h**), 3′-methyl- (compound **4k**), and 4′-phenyl-substituted (compound **4u**) APHAs displayed inhibitory activities similar to that of SAHA.

TSA was still a very potent inhibitor of HD1-A (IC_{50} = 0.8 nM),

Table 2. (Continued)

Compd	R	mp [°C]	Recrystallization Solvent	Yield [%]	Formula	Anal[a]
8o	4-NO_2	210–212	benzene/acetonitrile	76	$C_{16}H_{14}N_2O_5$	C, H, N
8p	3-OMe	150–152	benzene	69	$C_{17}H_{17}NO_4$	C, H, N
8q	4-OMe	174–176	benzene/acetonitrile	72	$C_{17}H_{17}NO_4$	C, H, N
8r	3-OEt	102–103	benzene	74	$C_{18}H_{19}NO_4$	C, H, N
8s	4-OEt	178–180	benzene/acetonitrile	83	$C_{18}H_{19}NO_4$	C, H, N
8t	3-Ph	135–136	benzene/acetonitrile	80	$C_{22}H_{19}NO_3$	C, H, N
8u	4-Ph	190–192	benzene/acetonitrile	73	$C_{22}H_{19}NO_3$	C, H, N
8v	3,5-Me_2	81–83	diethyl ether	87	$C_{18}H_{19}NO_3$	C, H, N
8w	3,5-F_2	238–239	benzene/acetonitrile	81	$C_{16}H_{13}F_2NO_3$	C, H, N, F
8x	3-NH_2	182–183	benzene	64	$C_{16}H_{16}N_2O_3$	C, H, N
8y	3-NHCOPh	182–183	benzene	75	$C_{23}H_{20}N_2O_4$	C, H, N
8z	3-$NHSO_2$Ph	81–83	diethyl ether	87	$C_{22}H_{20}N_2O_5S$	C, H, N, S
8a′	3-Cl-4-OMe	239–240	acetonitrile	62	$C_{17}H_{16}ClNO_4$	C, H, N, Cl

[a] Analytical results were within ±0.4% of theoretical values.

whereas SAHA exhibited sub-micromolar activity (IC_{50} = 0.2 μM), showing a 6.7-fold selectivity in favor of class I HDACs. In comparison with SAHA, nearly all APHA derivatives described herein were more potent in the inhibition of HD1-A, with the sole exceptions of the 2′-bromo (compound **4g**) and the 3′-phenyl (compound **4t**) derivatives.

Mouse HDAC1 inhibitory activity of selected compounds

Among the title compounds, the 3′-chloro (compound **4b**) and 3′-methyl (compound **4k**) derivatives were 2–7.5-fold more potent than **2** toward inhibition of the maize enzymes (HD2, HD1-B, and HD1-A). Thus, we tested the same compounds against mouse HDAC1 and compared the results with those of **2** and SAHA (Table 5). Similar to the data obtained with maize HD2, **4b** and **4k** were 2-fold more potent than **2**, and 2–3-fold less potent than SAHA in inhibiting mouse HDAC1.

Table 3. Maize HD2 Inhibitory Activity of Compounds **4a**–**a′**.[a]

Compd	R	Inhibition [%][b]	IC_{50} ± SD [μM]
4a	2-Cl	94.3 (24.1)	0.09 ± 0.004
4b	3-Cl	97.2 (24.1)	0.05 ± 0.001
4c	4-Cl	96.8 (24.1)	0.10 ± 0.005
4d	2-F	96 (25.4)	0.13 ± 0.006
4e	3-F	96.9 (25.4)	0.07 ± 0.003
4f	4-F	93.9 (25.4)	0.15 ± 0.007
4g	2-Br	91.1 (21.2)	0.18 ± 0.009
4h	3-Br	98 (21.2)	0.08 ± 0.004
4i	4-Br	93.7 (21.2)	0.15 ± 0.007
4j	2-Me	95 (25.8)	0.21 ± 0.01
4k	3-Me	96.6 (25.8)	0.06 ± 0.003
4l	4-Me	83 (1.3)	0.23 ± 0.009
4m	2-NO_2	96 (23.4)	0.16 ± 0.005
4n	3-NO_2	97 (23.4)	0.13 ± 0.005
4o	4-NO_2	97.2 (23.4)	0.18 ± 0.005
4p	3-OMe	96.5 (24.5)	0.07 ± 0.003
4q	4-OMe	93.7 (24.5)	0.06 ± 0.001
4r	3-OEt	91.2 (23.4)	0.34 ± 0.02
4s	4-OEt	93.6 (23.4)	0.18 ± 0.005
4t	3-Ph	95 (21.3)	0.25 ± 0.01
4u	4-Ph	97 (21.3)	0.09 ± 0.004
4v	3,5-Me_2	97 (23.4)	0.07 ± 0.003
4w	3,5-F_2	95 (24)	0.12 ± 0.004
4x	3-NH_2	88.5 (25.5)	1.84 ± 0.07
4y	3-NHCOPh	94.1 (19.1)	0.10 ± 0.002
4z	3-$NHSO_2$Ph	94.3 (17.5)	0.09 ± 0.003
4a′	3-Cl-4-OMe	95 (22.1)	0.08 ± 0.002
2[c]		96 (29)	0.10 ± 0.004
3[d]		98 (25.7)	0.05 ± 0.003
NaB		35 (5000)	ND[e]
VPA			128 ± 3.8
TSA			0.007 ± 0.0002
SAHA			0.05 ± 0.001
TPX			0.01 ± 0.0003
HC-toxin			0.11 ± 0.004
PAOA			292 ± 8.8
tubacin		92.9 (40)	2.0 ± 0.1

[a] Data represent mean values of at least three separate experiments. [b] At a fixed dose (μM). [c] Ref. [43]. [d] Ref. [44]. [e] Not determined.

Table 4. Inhibitory activities of compounds **4a**–**a′** toward maize HD1-B and HD1-A.[a]

Compd	R	IC_{50} ± SD [μM]		Fold Selectivity	
		HD1-B	HD1-A	Class I	Class II
4a	2-Cl	0.13 ± 0.005	0.12 ± 0.005		
4b	3-Cl	0.03 ± 0.0007	0.03 ± 0.001		
4c	4-Cl	0.07 ± 0.003	0.06 ± 0.002		
4d	2-F	0.04 ± 0.001	0.02 ± 0.0005		
4e	3-F	0.04 ± 0.001	0.03 ± 0.0005		
4f	4-F	0.06 ± 0.002	0.07 ± 0.003		
4g	2-Br	0.29 ± 0.015	0.21 ± 0.011		
4h	3-Br	0.04 ± 0.001	0.03 ± 0.001		
4i	4-Br	0.06 ± 0.002	0.05 ± 0.002		
4j	2-Me	0.10 ± 0.004	0.11 ± 0.004		
4k	3-Me	0.02 ± 0.0005	0.03 ± 0.0008		
4l	4-Me	ND[b]	ND		
4m	2-NO_2	0.07 ± 0.003	0.08 ± 0.003		
4n	3-NO_2	0.07 ± 0.003	0.13 ± 0.004		
4o	4-NO_2	0.06 ± 0.001	0.12 ± 0.005	2	
4p	3-OMe	0.05 ± 0.002	0.04 ± 0.001		
4q	4-OMe	0.06 ± 0.002	0.09 ± 0.004		
4r	3-OEt	0.15 ± 0.004	0.13 ± 0.005		
4s	4-OEt	0.06 ± 0.002	0.06 ± 0.002		
4t	3-Ph	1.16 ± 0.07	0.32 ± 0.013		3.6
4u	4-Ph	0.02 ± 0.0005	0.05 ± 0.002	2.5	
4v	3,5-Me_2	ND	ND		
4w	3,5-F_2	ND	ND		
4x	3-NH_2	ND	ND		
4y	3-NHCOPh	0.08 ± 0.004	0.05 ± 0.003		
4z	3-$NHSO_2$Ph	0.10 ± 0.006	0.05 ± 0.003		2
4a′	3-Cl-4-OMe	0.10 ± 0.006	0.04 ± 0.001		2.5
2		0.15 ± 0.004	0.05 ± 0.001		3
3		0.12 ± 0.006	0.06 ± 0.002		2
TSA		0.0004 ± 0.00001	0.0008 ± 0.00003	2	
SAHA		0.03 ± 0.001	0.2 ± 0.009	6.7	
PAOA		150 ± 4.5	756 ± 30.2	5	
tubacin		0.98 ± 0.04	0.45 ± 0.02		2.2

[a] Data represent mean values of at least three separate experiments. [b] Not determined.

Table 5. Inhibitory activities of compounds **4b** and **4k** toward mouse HDAC1.[a]

Compd	R	$IC_{50} \pm SD$ [μM]
4b	3-Cl	0.23 ± 0.01
4k	3-Me	0.31 ± 0.01
2[b]		0.51 ± 0.02
SAHA		0.11 ± 0.004

[a] Data represent mean values of at least three separate experiments. [b] Ref. [43].

Molecular modeling and docking studies

Homology models for the HD1-A[48,49,66] and HD1-B[46,47] sequences were derived by using the CPHmodels 2.0 Server[65] with structural data from the HDAC8–TSA complex[67] (PDB code: 1T64). The models were refined with a molecular dynamics (MD) protocol (Experimental Section) by using the program AMBER 8.0.[68,69]

The Autodock[70] program was used to explore the binding mode of derivatives **4u** and **4t**, the most selective derivatives against HD1-B and HD1-A, respectively. In general, the docked conformations obtained with the two enzymes differ mainly in that the molecules are placed deeper in the HD1-A pocket, where they partially occupy the acetyl escape channel,[71] whereas in HD1-B, the docked conformations adopt different conformations (Figure 4 and Figure 5).

Binding mode of 4u: The Autodock lowest-energy pose for derivative **4u** in HD1-A shows a deep position inside the catalytic channel (Supporting Information). Inspection of the binding mode reveals several positive interactions: the hydroxy oxygen atom is positioned within hydrogen-bonding distance from either the carbonyl oxygen atom of Ala 277 ($d = 2.62$ Å) or that of Pro 106 ($d = 2.73$ Å); the hydroxyamide carbonyl oxygen atom is within weak hydrogen-bonding distance from

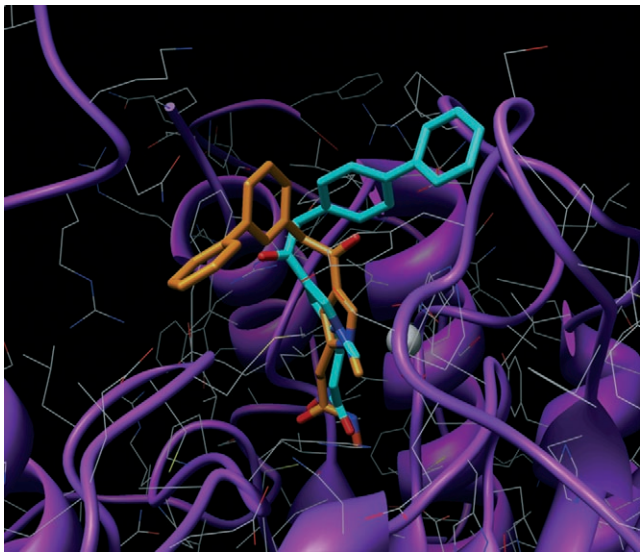

Figure 4. Derivatives **4t** (orange) and **4u** (cyan) docked into HD1-A. The enzyme is shown in tube representation (violet), and side chains are in gray.

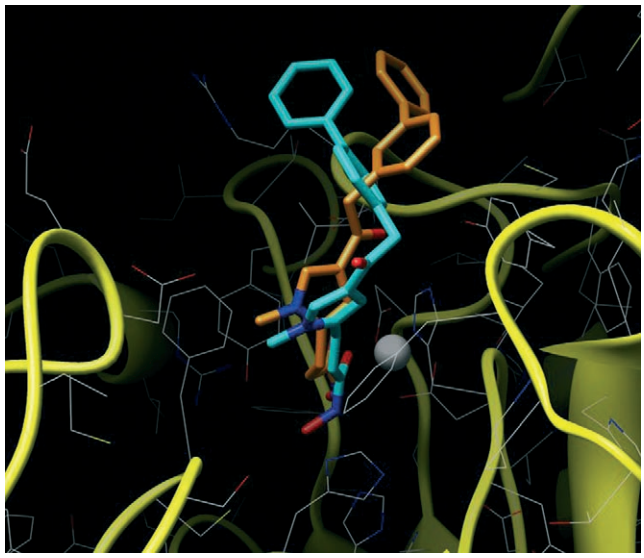

Figure 5. Derivatives **4t** (orange) and **4u** (cyan) docked into HD1-B. The enzyme is shown in tube representation (yellow), and side chains are in gray.

His 109 NH ($d = 3.20$ Å); a weak hydrogen bond is present between the phenylacetyl carbonyl oxygen atom and the phenol group of Tyr 180 (O–O distance = 3.74 Å). Finally, positive hydrophobic interactions (< 4 Å) are possible between the 4-biphenyl group of **4u** and the benzyl side chain of Tyr 180 and one of the methyl groups of Leu 249.

In contrast to HD1-A, the acetyl escape is narrower in the HD1-B model and places the hydroxyamide portion of **4u** close to the catalytic zinc ion (Supporting Information). This scenario reveals that the hydroxyamide carbonyl oxygen approaches the zinc ion at an effective chelating distance (Zn^{2+}···O=C $d = 1.88$ Å) that could explain the slightly improved selectivity toward HD1-B. Along with the chelation, further contributing interactions can be observed: the hydroxy oxygen atom is positioned within a weak hydrogen-bonding distance from the carbonyl oxygen atom of Gly 268 ($d = 3.87$ Å); the hydroxyamide nitrogen atom at a hydrogen-bonding distance from the carbonyl oxygen atom of Asp 144 ($d = 2.90$ Å). Furthermore, positive hydrophobic interactions may take place between the pyrrole group of **4u** and the benzyl side chain of Phe 173, and between the 4-phenyl substituent of **4u** and the side chain of Arg 238.

Binding mode of 4t: Similar to **4u**, the lowest-energy docked conformation of **4t** is placed deep inside the HD1-A catalytic tunnel (Supporting Information), and the pyrrolyl hydroxypropenamide moiety is nicely superimposed with that of **4u** (with some slight differences), whereas the biphenyl group of **4u** is swiveled ≈110°. This rotation of the biphenyl group leads to the disruption of the previously observed hydrophobic interactions for **4u** and creates new interactions with the Phe 118 side chain. In contrast to **4u**, the hydroxyamide group is rotated roughly 180°, and only weak hydrogen-bond interactions are displayed between the hydroxy oxygen atom and the carbonyl oxygen atom of Asp 149 ($d = 3.59$ Å), and between

the hydroxyamide carbonyl oxygen atom and the amide group of His 109 ($d = 3.79$ Å).

The lowest-energy docked conformation of **4t** in HD1-B is shifted back from the catalytic channel with an overall decrease in the contributing favorable interactions that could explain the slight selectivity of **4t** toward HD1-A. Moreover, comparison of the binding mode of **4t** with that of **4u** in the HD1-B catalytic pocket shows that whereas the latter is placed optimally to chelate Zn^{2+}, the former does not show any effective chelating distance between the hydroxyamide group and the zinc ion (Zn···O=C $d = 2.76$ Å, Zn···O–N $d = 3.02$ Å; Supporting Information).

Antiproliferative and cytodifferentiation activities of 4b on human acute promyelocytic leukemia HL-60 cells

Among the APHA derivatives showing the highest inhibitory values against the three maize enzymes (the 3′-substituted phenylacetylpyrroles **4b**,**e**,**h**,**k**,**p**), we chose 3[4-(3′-chlorophenylacetyl)-1-methyl-1*H*-pyrrol-2-yl]-*N*-hydroxy-2-propenamide (**4b**) to investigate its antiproliferative and cytodifferentiation properties in human acute promyelocytic leukemia HL-60 cells.

Antiproliferative effect: The capability of **4b** to inhibit the growth of the human leukemia cell line was evaluated in comparison with TSA (30 nM). Figure 6a shows the effect of **4b** on the growth of HL-60 cells cultured for 96 h with different compound concentrations. The APHA compound **4b** showed a significant dose-dependent inhibitory effect on the growth rate of the cell line. In particular, the growth curve of cells is inhibited in the presence of **4b** at concentrations of 2.5, 5, 10, and 20 μM by 15% ($p < 0.05$), 36% ($p < 0.01$), 49% ($p < 0.01$), and 86% ($p < 0.01$), respectively, relative to vehicle (Figure 6a). This inhibitory effect of **4b** does not appear to depend on a direct cytotoxic action of the drug. In fact, the viability index (VI) is significantly modified by **4b** at only 20 μM (VI = 64%, Figure 6b).

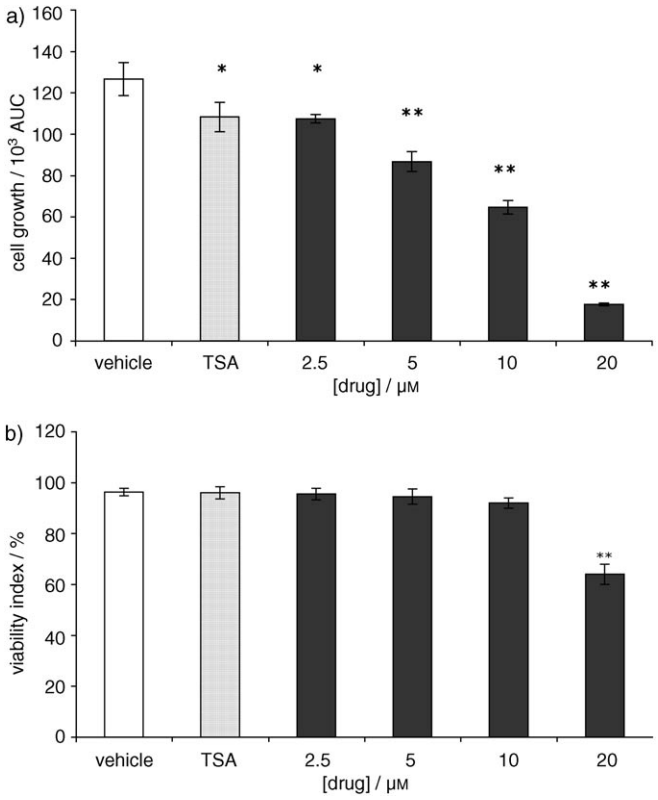

Figure 6. a) Effect of various concentrations of **4b** (in dark grey) on the growth of human leukemia cells cultured for 96 h in comparison with TSA (30 nM); data are expressed as cell number (mean ± SEM, $n = 4$); *$p < 0.05$, **$p < 0.01$. b) Cytotoxic effect in human leukemia cells cultured for 96 h with various concentrations of **4b** (in dark grey); each point represents the mean ± SEM ($n = 4$); **$p < 0.01$.

Differentiation activity: The restoration of so-called respiratory burst was evaluated as a fundamental functional marker of differentiation in human leukemia cell lines. This aspect of the phagocyte oxidative metabolism was analyzed by chemiluminescence (CL) in HL-60 cells incubated with various concentrations of **4b** for 96 h, followed by stimulation with phorbol-12-myristate-13-acetate (PMA). In particular, the presence of PMA-induced CL seems to demonstrate an acquired correct assembly of the NADPH oxidase system. The results clearly show a dose-dependent recovery of reactive oxygen species (ROS) metabolism when the cells upon cell stimulation with PMA; maximal CL activity ($p < 0.01$) was reached at a concentration of **4b** of 20 μM (Figure 7).

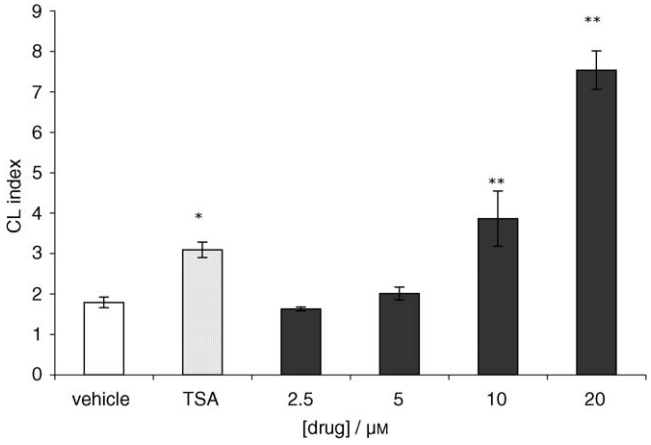

Figure 7. Concentration-dependent effect of **4b** on the differentiation of HL-60 cells with TSA (30 nM) as a reference. Cells were cultured with various concentrations of **4b** (in dark grey) for 96 h. Differentiation-inducing activity was measured by chemiluminescence (CL) as described in the Experimental Section. Each point represents the mean ± SEM ($n = 4$); *$p < 0.05$; **$p < 0.01$.

Conclusions

A new series of aroyl-pyrrolyl hydroxyamides (compounds **4**–**4a**′) have been described and are analogues of the lead compound 3-(1-methyl-4-phenylacetyl-1*H*-pyrrol-2-yl)-*N*-hydroxy-2-propenamide (**2**). The phenyl ring of **2** was substituted with a wide range of electron-donating and electron-withdrawing groups, and the effects were evaluated with three maize histone deacetylases: HD2, HD1-B (class I HDAC), and HD1-A (class II HDAC).

HD2 inhibition data (Table 3) shows that the insertion of substituents such as halogen or methyl groups at the 3′ posi-

tion of the benzene ring increases the inhibitory effect of the derivatives **4b**, **4e**, **4h**, and **4k** up to 2-fold. The highest inhibiting activity was showed by the 3-[4-(3′-chlorophenylacetyl)-1-methyl-1*H*-pyrrol-2-yl]-*N*-hydroxy-2-propenamide (**4b**, IC_{50} = 0.05 μM) and its 3′-methyl analogue **4k** (IC_{50} = 0.06 μM), which were more potent than VPA, HC-toxin, and **2**. Moreover, they showed the same activity as SAHA and were 7–5-fold less active than TSA and TPX. In assays against mouse HDAC1 in comparison with **2**, **4b** and **4k** showed inhibition data in agreement with those obtained in the anti-HD2 assay.

Assays for the inhibition of HD1-B and HD1-A (Table 4) performed with **4a**–**4a′** confirmed the inhibition trend observed with HD2 above. The introduction of various substituents at the 3′ and, to a lesser extent, at the 4′ positions of the benzene ring of **2** led to compounds up to 6-fold more active than **2** against HD1-B (with the exception of the 3′-ethoxy and 3′-phenyl compounds **4r** and **4t**), whereas their anti-HD1-A activity remained the same as **2**. The 3- and 2-fold selectivity ratios toward class II (HD1-A) enzymes displayed by **2** and **3**, respectively, was lost by the insertion of substituents at the benzene ring; exceptions include the 3′-phenyl (compound **4t**), 3′-benzenesulfonamido (compound **4z**), and the 3′-chloro-4′-methoxy (compound **4a′**) derivatives, which showed selectivity ratios from 2 to 3.6 in favor of class II. Two compounds, the 4-nitro and the 4-phenyl derivatives **4o** and **4u** displayed an opposite pattern of HD1-B/HD1-A inhibition, as both are slightly more potent against HD1-B than HD1-A. Molecular modeling studies based on HD1-B and HD1-A homology models have been performed to gather insight on the observed inhibition differences. In tests with human acute promyelocytic leukemia HL-60 cells, **4b** showed interesting, dose-dependent antiproliferative and cytodifferentiation properties.

Experimental Section

Chemistry: Melting points were determined on a Büchi 530 melting point apparatus and are uncorrected. IR spectra (KBr) were recorded on a Perkin–Elmer Spectrum One instrument. ^{1}H NMR spectra were recorded at 200 MHz on a Bruker AC 200 spectrometer; chemical shifts are reported in δ (ppm) relative to the internal reference tetramethylsilane (Me_4Si). All compounds were routinely checked by TLC and ^{1}H NMR. TLC was performed on aluminum-backed silica gel plates (Merck DC-Alufolien Kieselgel 60 F_{254}) with spots visualized by UV light. All solvents were reagent grade and, when necessary, were purified and dried by standard methods. The concentration of solutions after reactions and extractions involved the use of a rotary evaporator operating at a decreased pressure of ≈20 Torr. Organic solutions were dried over anhydrous sodium sulfate. Analytical results are within ±0.40% of the theoretical values. A sample of SAHA for biological assays was prepared as previously reported by us.[72] All chemicals were purchased from Aldrich Chimica, Milan (Italy) or Lancaster Synthesis GmbH, Milan (Italy) and were of the highest purity.

3-Biphenylacetic acid (5a): An aqueous solution of 2 M sodium carbonate (28.2 mmol, 3.0 g dissolved in 14 mL water) was added to a mixture of phenylboronic acid (13.4 mmol, 1.6 g) and methyl 3-bromophenylacetate (13.4 mmol, 3.1 g) dissolved in toluene/ethanol (35:3 *v/v*). After the resulting mixture was degassed for 10 min with nitrogen, tetrakis(triphenylphosphine)palladium (0.7 mmol, 0.8 g) was added, and the reaction was heated at 80 °C for 16 h. Afterward, it was cooled to room temperature, the suspension was filtered, and the solvent was evaporated under decreased pressure. The residue was partitioned between water (50 mL) and ethyl acetate (50 mL), the organic layer was separated, and the aqueous layer was extracted with ethyl acetate (2×50 mL). The organic layer was washed with brine (3×50 mL), dried, and concentrated in vacuo. The residue was purified by column chromatography on silica gel by eluting with ethyl acetate/chloroform 1:1. The crude methyl 3-biphenylacetate was then dissolved in ethanol and treated with 2 N KOH (26.9 mmol, 1.5 g, 13.5 mL). After stirring at room temperature for 5 h, the solution was poured into water (100 mL), and extracted with ethyl acetate (2×50 mL). A sample of 2 N HCl was added to the aqueous layer to reach pH 2, and the precipitate was filtered and purified by crystallization. ^{1}H NMR ($CDCl_3$): δ = 3.42 (s, 2H, CH_2), 7.05 (m, 1H, benzene H-4′), 7.17 (m, 1H, benzene H-6), 7.30 (m, 5H, benzene H-5,2′,3′,5′,6′), 7.47 (m, 2H, benzene H-2,4), 8.55 ppm (br s, 1H, OH). Anal. ($C_{14}H_{12}O_2$) C, H.

3-Chloro-4-methoxyphenylacetic acid (5b): Potassium peroxymonosulfate (oxone) (12.0 mmol, 7.4 g) was added to a solution of 4-methoxyphenylacetic acid (12.0 mmol, 2.0 g) dissolved in acetone (20 mL), and the suspension was stirred at room temperature for 15 min. Afterward, an aqueous solution of sodium chloride (48.1 mmol, 2.8 g, 20 mL) was added, and the resulting mixture was stirred for 6 h. When the reaction was finished (TLC control: SiO_2/ethyl acetate), the solvent was evaporated under decreased pressure, and the residue was diluted with water (100 mL) and extracted with ethyl acetate (3×50 mL). The organic layer was washed with sodium chloride solution (3×50 mL), dried, and concentrated. The residue was a solid that was recrystallized with cyclohexane/benzene. ^{1}H NMR ($CDCl_3$): δ = 3.56 (s, 2H, CH_2), 3.87 (s, 3H, CH_3), 6.88 (m, 1H, benzene H-5), 7.14 (m, 1H, benzene H-6), 7.30 (m, 1H, benzene H-2), 9.00 ppm (br s, 1H, OH). Anal. ($C_9H_9ClO_3$) C, H, Cl.

General procedure for 4-aroyl-1-methyl-1*H*-pyrrole-2-carboxaldehydes 6a–w; example: 4-(4′-methylphenylacetyl)-1-methyl-1*H*-pyrrole-2-carboxaldehyde (6l): A solution of oxalyl chloride (18.4 mmol, 1.4 mL) in 1,2-dichloroethane (20 mL) was added to a cooled (0–5 °C) solution of *N*,*N*-dimethylformamide (18.4 mmol, 1.6 mL) in 1,2-dichloroethane (20 mL) over a period of 5–10 min. After stirring at room temperature for 15 min, the suspension was cooled (0–5 °C) again and treated with a solution of 1-methyl-1*H*-pyrrole (18.4 mmol, 1.5 g) in 1,2-dichloroethane (20 mL). The mixture was stirred at room temperature for 15 min, and was then treated with aluminum trichloride (40.6 mmol, 5.4 g) and 4-tolylacetyl chloride (previously prepared by heating the corresponding acid (18.4 mmol, 2.8 g) with $SOCl_2$ (20 mL) for 1 h at 50 °C). After 3 h, the reaction mixture was poured onto crushed ice (100 g) containing 50% NaOH (20 mL) and was stirred for 10 min. The solution was adjusted to pH 4 with 37% HCl, the organic layer was separated, and the aqueous layer was extracted with chloroform (2× 20 mL). The combined organic solutions were washed with water (3×50 mL), dried, and evaporated to dryness. The residual oil was purified by column chromatography on silica gel, eluting with ethyl acetate/chloroform (1:5). The solid obtained was recrystallized from cyclohexane/benzene to give pure **6l**. ^{1}H NMR ($CDCl_3$): δ = 2.27 (s, 3H, $PhCH_3$), 3.90 (s, 3H, NCH_3), 3.96 (s, 2H, $PhCH_2CO$), 7.10 (dd, 4H, benzene H), 7.27 (d, 1H, pyrrole H^{β}), 7.39 (d, 1H, pyrrole H^{α}), 9.54 ppm (s, 1H, CHO). Anal. ($C_{15}H_{15}NO_2$) C, H, N.

General procedure for ethyl 3-(4-aroyl-1-methyl-1*H*-pyrrol-2-yl)-2-propenoates 7a–w; example: ethyl 3-[4-(3′-methoxyphenyl-

acetyl)-1-methyl-1*H*-pyrrol-2-yl]-2-propenoate (7p): A suspension of **6p** (1.7 mmol, 0.6 g) in absolute ethanol (20 mL) was added in one portion to a mixture of triethyl phosphonoacetate (2.1 mmol, 0.4 mL) and anhydrous potassium carbonate (3.5 mmol, 0.5 g). After stirring at 70 °C for 2 h, the reaction mixture was cooled to room temperature, diluted with water (50 mL), and extracted with ethyl acetate (3×50 mL). The organic layer was washed with water, dried, and evaporated to dryness, and the solid residue was recrystallized to furnish pure **7p**. ^{1}H NMR ($CDCl_3$): $\delta = 1.36$ (t, 3H, $COOCH_2CH_3$), 3.74 (s, 3H, NCH_3), 3.81 (s, 3H, OCH_3), 4.01 (s, 2H, CH_2CO), 4.27 (q, 2H, $COOCH_2CH_3$), 6.25 (d, 1H, CH=CHCO), 6.90 (m, 3H, benzene H-2,4,6), 7.10 (m, 1H, pyrrole H^β), 7.26 (m, 1H, benzene H-5), 7.40 (m, 1H, pyrrole H^α), 7.55 ppm (d, 1H, CH=CHCO). Anal. ($C_{19}H_{21}NO_4$) C, H, N.

Ethyl 3-[4-(3′-aminophenylacetyl)-1-methyl-1*H*-pyrrol-2-yl]-2-propenoate (7x): Potassium carbonate (4.1 mmol, 0.6 g) and 10% palladium on carbon (20 mg) were slowly added to a solution of ethyl 3-[4-(3′-nitrophenylacetyl)-1-methyl-1*H*-pyrrol-2-yl]-2-propenoate **7n** (5.8 mmol, 2.0 g) in a mixture of water (4 mL) and THF (5 mL). After stirring at room temperature for 10 min, a solution of sodium hypophosphite (22.2 mmol, 2.4 g) in water (30 mL) was added. After stirring at room temperature for 2 h, the reaction mixture was filtered, the organic layer was separated, and the aqueous layer was extracted with ethyl acetate (3×50 mL). The combined organic solution was washed with water (2×100 mL), dried, and evaporated to dryness. The residual oil was purified with column chromatography on silica gel by eluting with a mixture of ethyl acetate and chloroform (1:1). Compound **7x** was obtained as a pure oil. ^{1}H NMR ($CDCl_3$): $\delta = 1.30$ (t, 3H, $COOCH_2CH_3$), 3.72 (s, 3H, NCH_3), 3.90 (s, 2H CH_2CO), 4.24 (q, 2H, $COOCH_2CH_3$), 6.25 (d, 1H, CH=CHCO), 6.38 (d, 1H, pyrrole H^β), 6.64 (m, 2H, NH_2), 6.70 (m, 3H, benzene H-2,4,6), 7.09 (m, 1H, benzene H-5), 7.36 (m, 1H, pyrrole H^α), 7.49 ppm (d, 1H, CH=CHCO). Anal. ($C_{18}H_{20}N_2O_3$) C, H, N.

General procedure for ethyl 3-[4-(3′-benzoyl- and 3-[4-(3′-benzenesulfonylaminophenylacetyl)-1-methyl-1*H*-pyrrol-2-yl]-2-propenoates 7y,z; example: ethyl 3-[4-(3′-benzenesulfonylaminophenylacetyl)-1-methyl-1*H*-pyrrol-2-yl]-2-propenoate (7z): Benzenesulfonyl chloride (6.8 mmol, 2.1 g) and triethylamine (10.2 mmol, 1.4 mL) were added to a solution of 3-[4-(3′-aminophenylacetyl)-1-methyl-1*H*-pyrrol-2-yl]-2-propenoate (**7x**) (6.8 mmol, 2.1 g) in dichloromethane (20 mL). After stirring at room temperature for 1 h, the reaction mixture was poured into water (50 mL), the organic layer was separated, and the aqueous layer was extracted with chloroform (2×50 mL). The combined organic solution was washed with water (100 mL) and brine (100 mL), dried, and evaporated to dryness. The residual oil was purified with column chromatography on silica gel by eluting with a mixture of ethyl acetate and chloroform (1:1). Compound **7z** was obtained as a pure oil. ^{1}H NMR ($CDCl_3$): $\delta = 1.28$ (t, 3H, $COOCH_2CH_3$), 3.72 (s, 3H, NCH_3), 3.90 (s, 2H CH_2CO), 4.20 (q, 2H, $COOCH_2CH_3$), 6.25 (d, 1H, CH=CHCO), 6.90–7.95 ppm (m, 12H, pyrrole protons, benzene protons, and CH=CHCO). Anal. ($C_{24}H_{24}N_2O_5S$) C, H, N, S.

Ethyl 3-[4-(3′-chloro-4′-methoxyphenylacetyl)-1-methyl-1*H*-pyrrol-2-yl]-2-propenoate (7a′): Aluminum trichloride (15.0 mmol, 2.0 g) was slowly added to a cooled (0–5 °C) solution of ethyl (1-methyl-1*H*-pyrrol-2-yl)-2-propenoate[53] (7.5 mmol, 1.3 g) and 3-chloro-4-methoxyphenylacetyl chloride (previously prepared by heating **5b** (15.0 mmol, 3.0 g) with $SOCl_2$ (20 mL) for 1 h at 50 °C) in 1,2-dicloroethane (100 mL). After stirring at room temperature for 30 min, the reaction mixture was poured onto crushed ice (100 g), and the solution was adjusted to pH 4 with 37% HCl. The organic layer was separated, and the aqueous layer was extracted with chloroform (3×50 mL). The combined organic solution was washed with water (100 mL), dried, and evaporated to dryness. The residual oil was purified with column chromatography on silica gel by eluting with a mixture of ethyl acetate and chloroform (1:20). Compound **7a′** was obtained as a pure solid. ^{1}H NMR ($CDCl_3$): $\delta = 1.32$ (t, 3H, $COOCH_2CH_3$), 3.71 (s, 3H, NCH_3), 3.87 (s, 3H, OCH_3), 3.93 (s, 2H CH_2CO), 4.25 (q, 2H, $COOCH_2CH_3$), 6.25 (d, 1H, CH=CHCO), 6.88 (m, 1H, benzene H-5), 7.03 (m, 1H, pyrrole H^β), 7.13 (m, 2H, benzene H-6), 7.30 (m, 1H, benzene H-2), 7.35 (m, 1H, pyrrole H^α), 7.52 ppm (d, 1H, CH=CHCO). Anal. ($C_{19}H_{20}ClNO_4$) C, H, Cl, N.

General procedure for 3-(4-aroyl-1-methyl-1*H*-pyrrol-2-yl)-2-propenoic acids 8a–a′: example: 3-[4-(4′-chlorophenylacetyl)-1*H*-pyrrol-2-yl)]-2-propenoic acid (8c): A mixture of **7c** (4.3 mmol, 1.4 g), 2 N KOH (17.2 mmol, 1.0 g, 8.6 mL), and ethanol (15 mL) was stirred at room temperature overnight. Afterward, the solution was poured into water (50 mL) and extracted with ethyl acetate (3× 20 mL). HCl (2 N) was added to the aqueous layer to reach pH 5, and the precipitate obtained was filtered and recrystallized from benzene/acetonitrile to give the pure compound **8c**. ^{1}H NMR ([D_6]DMSO): $\delta = 3.70$ (s, 3H, NCH_3), 3.98 (s, 2H, CH_2CO), 6.25 (d, 1H, CH=CHCO), 7.28 (m, 6H, benzene and pyrrole protons), 7.40 (d, 1H, CH=CHCO), 12.10 ppm (br s, 1H, OH). Anal. ($C_{16}H_{14}ClNO_3$) C, H, Cl, N.

General procedure for 3-(4-aroyl-1-methyl-1*H*-pyrrol-2-yl)-*N*-hydroxy-2-propenamides 4a–a′; example: 3-[4-(2′-fluorophenylacetyl)-1-methyl-1*H*-pyrrol-2-yl]-*N*-hydroxy-2-propenamide (4d): Ethyl chloroformate (1.9 mmol, 0.2 mL) and triethylamine (2.0 mmol, 0.3 mL) were added to a cooled (0 °C) solution of **3d** (1.6 mmol, 0.5 g) in dry THF (10 mL), and the mixture was stirred for 10 min. The solid was filtered off, and *O*-(2-methoxy-2-propyl)-hydroxyamine (4.7 mmol, 0.4 mL)[54] was added to the filtrate. The solution was stirred for 15 min at 0 °C, evaporated under decreased pressure, and the residue was diluted in methanol (10 mL). Amberlyst 15 ion-exchange resin (0.2 g) was added to the solution of the *O*-protected hydroxamate, and the mixture was stirred at 45 °C for 1 h. Afterward, the reaction was filtered, and the filtrate was concentrated in vacuo to give the crude **4d**, which was purified by crystallization. ^{1}H NMR ([D_6]DMSO): $\delta = 3.78$ (s, 3H, NCH_3), 4.15 (s, 2H, CH_2CO), 6.33 (d, 1H, CH=CHCO), 6.99 (m, 1H, pyrrole H^β), 7.38 (m, 5H, benzene protons and CH=CHCO), 7.80 (m, 1H, pyrrole H^α), 9.01 (br s, 1H, NH), 10.72 ppm (br s, 1H, OH). Anal. ($C_{16}H_{15}FN_2O_3$) C, H, F, N.

In vitro inhibition assays of maize HD2, HD1-B, and HD1-A: Radioactively labeled chicken core histones were used as the enzyme substrate according to established procedures.[55–58] The enzyme liberated tritiated acetic acid from the substrate, which was quantified by scintillation counting. IC_{50} values are the results of triple determinations. A sample of maize enzyme (50 μL at 30 °C) was incubated for 30 min with 10 μL total [^{3}H]acetate-prelabeled chicken reticulocyte histones (1 mg mL^{-1}). The reaction was stopped by the addition of 1 M HCl/0.4 M acetate (36 μL) and ethyl acetate (800 μL). After centrifugation (10000 *g*, 5 min), an aliquot (600 μL) of the upper phase was counted for radioactivity in liquid scintillation cocktail (3 mL). The compounds were tested at a starting concentration of 40 μM, and active substances were diluted further. NaB, VPA, TSA, SAHA,[72] TPX, HC-toxin, PAOA, and tubacin were used as reference compounds, and blank solvents were used as negative controls.

Mouse HDAC1 enzyme assay: HDAC1 from mouse A20 cells (ATCC: TIB-208) partially purified by anion-exchange and affinity

chromatography was used as the enzyme source. HDAC activity was determined as described[73] by using [^{3}H]acetate-prelabeled chicken reticulocyte histones as substrate. Mouse HDAC1 (50 μL) was incubated with various concentrations of compounds for 15 min on ice; total [^{3}H]acetate-prelabeled chicken reticulocyte histones (10 μL, 4 mg mL^{-1}) were added to give a final concentration of 41 μM. The mixture was incubated at 37 °C for 1 h. The reaction was stopped by the addition of 1 M HCl/0.4 M acetylacetate (50 μL) and 1 mL ethyl acetate. After centrifugation at 10000 *g* for 5 min, an aliquot (600 μL) of the upper phase was counted for radioactivity in 3 mL liquid scintillation cocktail.

Homology models, molecular modeling, and docking studies:

HD1-A and HD1-B 3D model preparation: Class I (HD1-B) and class II (HD1-A) HDAC homologue structures were prepared with the sequences deposited in the TrEMBL Protein Database (entry codes P56521 for HD1-B and Q7XAX9 for HD1-A). The homology models were automatically obtained by feeding the CPHmodels 2.0 Server[65] with the above sequences and using the HDAC8–TSA complex as template (PDB code: 1T64) (Supporting Information). The two models were then refined by the AMBER 8.0 program with the following protocol: first, the experimental bound conformation of TSA as found in the template was merged into either the HD1-A or HD1-B complex. AM1-BCC charges were calculated on TSA, employing the antechamber module of AMBER 8.0.[74] Through use of the xLeap AMBER module, hydrogen atoms were added to the starting complexes. The complexes were then solvated in an octahedral box of Monte Carlo TIP3P water with each box side at least 10.0 Å away from the nearest atoms of the complexes. Sodium ions were included to neutralize the charge of the system. The ions were placed randomly (by replacement of water molecules) in the system 10 Å away from each other and from the nearest atoms. The hydrogen atoms, counterions, and water molecules were then minimized over 1000 iterations. Then, the whole complexes were relaxed over 5000 iterations. The MD simulations were performed with the smooth particle-mesh Ewald (PME) method to accommodate long-range electrostatic forces and with periodic boundary conditions at constant volume. The simulations used the AMBER all-atom (parm99) and the GAFF force fields with a step size of 2 fs. By using an extended list technique, the non-bonded interactions were effectively updated every step with a small overhead in computational cost. The non-bonded cut-off for van der Waals interactions was set to 10 Å. All covalent bonds involving hydrogen atoms were constrained by using SHAKE. The ions and water molecules were then equilibrated for 20 ps at constant volume followed by energy minimization while freezing the model complex. Then a second equilibration was carried out for 90 ps while gradually unfreezing the bound TSA. A final equilibration for a further 150 ps was carried out on the whole complexes without any restraint. During the equilibrations the stability of the complexes was monitored through their root mean square deviations (rmsd) (Supporting Information). By the mean of the ptraj module in AMBER, the average structures were obtained from the last part of the equilibrations and were energy-minimized over 1000 iterations. Deletions of the bound TSA molecules led to the HD1-A and HD1-B models used for the subsequent docking studies.

Docking of 4t and 4u: The docking studies were performed with Autodock 3.0.5. The molecular structures of derivatives **4t** and **4u** were drawn with the PRODGR software,[75] which provides the molecule ready for direct use by Autodock. The AutodockTools package was employed to generate the docking input files and to analyze the docking results; the procedure described in the manual was followed. All water molecules and nonpolar hydrogen atoms were removed. The Kollmann charges were loaded for the proteins while the charges applied by the PRODRG program were retained in the ligand. A grid box size of 40×40×60 points with a spacing of 0.375 Å between grid points was implemented and covered most of the catalytic channel of either enzyme. The center of mass of the bound TSA was used for the grid origin. For all inhibitors, the single bonds including the amide bonds were treated as active torsional bonds. One hundred structures, (30 runs) were generated by using genetic algorithm searches. A default protocol was applied with an initial population of 50 randomly placed individuals, a maximum number of 2.5×10^5 energy evaluations, and a maximum number of 2.7×10^4 generations. A mutation rate of 0.02 and a crossover rate of 0.8 were used. In a parallel docking experiment, the bound TSA molecules extracted from either average MD-equilibrated complex were docked back. Autodock proved to reposition the TSA with a minimal rmsd error ($rmsd_{TSA-HD1-A}=1.29$, $rmsd_{TSA-HD1-B}=0.95$).

Growth inhibition and cell differentiation assays:

Cell culture and reagents: Human acute promyelocytic leukemia HL-60 cells were obtained from the Interlab Cell Line Collection (CBA, Genoa, Italy). Cells were maintained at 37 °C under a humidified atmosphere of 5% CO_2 in RPMI 1640 HEPES-modified medium supplemented with 10% (*v/v*) heat-inactivated fetal calf serum, glutamine (2 mmol L^{-1}), penicillin (100 IU mL^{-1}), and streptomycin (100 μg mL^{-1}). Unless otherwise indicated, all chemicals and reagents (cell culture grade) were obtained from Sigma Chemical Co., Milan, Italy.

Cell viability and growth inhibition assays: Cell number was determined with a Neubauer hemocytometer, and viability was assessed by the ability of the cells to exclude trypan blue. The stock solutions were prepared immediately before use. TSA and **4b** were dissolved in DMSO. HL-60 exponentially growing cells (2×10^5 cells mL^{-1}) were set at day 0 in media containing various concentrations of drugs for 96 h. The final concentrations of the drugs were as follows: TSA: 30 nM; **4b**: 2.5, 5, 10, and 20 μM. The final concentration of DMSO, used as a vehicle, was the same (0.1% *v/v*) in all samples during the experiments.

Cell differentiation assay: The stimulated production of reactive oxygen species (ROS) by phorbol-12-myristate-13-acetate (PMA) which is mostly due to the activity of the NADPH oxidase system, was used as a marker of differentiation in the human myeloid cell line HL-60. ROS metabolism was studied by a chemiluminescence (CL) assay as already described.[76] Briefly, assays were performed in triplicate in an automatic luminometer (Autolumat LB 953, EG&G, Turku, Finland) at 25 °C for 120 min with cycles of 5 min each. The CL system contained 1×10^5 cells, luminol (100 nmol), PMA (150 pmol), and was either left without treatment (control), treated with 0.1% DMSO (vehicle alone), or treated with various differentiating factors, and adjusted to a final volume of 1.0 mL with KRP solution. Unstimulated activity was measured in the absence of stimulus. Stimulated CL was evaluated through the calculation of the CL index: $(AUC_{stimulated\ cells})/(AUC_{unstimulated\ cells})$, in which AUC (area under curve) is expressed as (counts) (cell)$^{-1}$ (120 min)$^{-1}$.

Statistical analysis: All results are expressed as the mean ± SEM. The group mean values were compared by the analysis of variance (ANOVA) followed by a multiple comparison of means by the Dunnet test; $p<0.05$ was considered significant.

Acknowledgement

The authors thank Dr. Jason C. Wong (Harvard University, Cambridge, MA) for the kind gift of tubacin. This work was supported by grants from "Progetto Finalizzato Ministero della Salute 2002", "AIRC Proposal 2005", and PRIN 2004.

Keywords: aroyl-pyrrolyl hydroxyamides · cytodifferentiation · enzymes · histone deacetylase · inhibitors

[1] C. A. Hassig, S. L. Schreiber, *Curr. Opin. Chem. Biol.* **1997**, *1*, 300 – 308.
[2] T. Kouzarides, *Curr. Opin. Genet. Dev.* **1999**, *9*, 40 – 48.
[3] B. D. Strahl, C. D. Allis, *Nature* **2000**, *403*, 41 – 45.
[4] J. Wu, M. Grunstein, *Trends Biochem. Sci.* **2000**, *25*, 619 – 623.
[5] M. Grunstein, *Nature* **1997**, *389*, 349 – 352.
[6] S. Khochbin, A. Verdel, C. Lemercier, D. Seigneurin-Berny, *Curr. Opin. Genet. Dev.* **2001**, *11*, 162 – 166.
[7] S. K. Kurdistani, M. Grunstein, *Nat. Rev. Mol. Cell Biol.* **2003**, *4*, 276 – 284.
[8] K. Luger, A. W. Mäder, R. K. Richmond, D. F. Sargent, T. J. Richmond, *Nature* **1997**, *389*, 251 – 260.
[9] F. D. Urnov, A. Wolffe, *Emerging Ther. Targets* **2000**, *4*, 665 – 685.
[10] W. Fischle, Y. Wang, C. D. Allis, *Curr. Opin. Cell Biol.* **2003**, *15*, 172 – 183.
[11] C. W. Akey, K. Luger, *Curr. Opin. Struct. Biol.* **2003**, *13*, 6 – 14.
[12] P. A. Jones, S. B. Baylin, *Nat. Rev. Genet.* **2002**, *3*, 415 – 428.
[13] R. L. Momparler, *Oncogene* **2003**, *22*, 6479 – 6483.
[14] C. Huang, E. A. Sloan, C. F. Boerkoel, *Curr. Opin. Genet. Dev.* **2003**, *13*, 246 – 252.
[15] M. Verma, S. Srivastava, *Lancet Oncol.* **2002**, *3*, 755 – 763.
[16] U. H. Weidle, A. Grossmann, *Anticancer Res.* **2000**, *20*, 1471 – 1486.
[17] O. H. Kramer, M. G. Göttlicher, T. Heinzel, *Trends Endocrinol. Metab.* **2001**, *12*, 294 – 300.
[18] P. A. Marks, V. M. Richon, R. Breslow, R. A. Rifkind, *Curr. Opin. Oncol.* **2001**, *13*, 477 – 483.
[19] P. A. Marks, R. A. Rifkind, V. M. Richon, R. Breslow, T. Miller, W. K. Kelly, *Nat. Rev. Cancer* **2001**, *1*, 194 – 202.
[20] D. M. Vigushin, R. C. Coombes, *Anti-Cancer Drugs* **2002**, *13*, 1 – 13.
[21] R. W. Johnstone, *Nat. Rev. Drug Discovery* **2002**, *1*, 287 – 299.
[22] W. K. Kelly, O. A. O'Connor, P. A. Marks, *Expert Opin. Invest. Drugs* **2002**, *11*, 1695 – 1713.
[23] T. A. Miller, D. J. Witter, S. Belvedere, *J. Med. Chem.* **2003**, *46*, 5097 – 5116.
[24] A. Mai, S. Massa, D. Rotili, I. Cerbara, S. Valente, R. Pezzi, S. Simeoni, R. Ragno, *Med. Res. Rev.* **2005**, *25*, 261 – 309.
[25] C. M. Grozinger, S. L. Schreiber, *Chem. Biol.* **2002**, *9*, 3 – 16.
[26] A. Lusser, G. Brosch, A. Loidl, H. Haas, P. Loidl, *Science* **1997**, *277*, 88 – 91.
[27] J. M. Denu, *Trends Biochem. Sci.* **2003**, *28*, 41 – 48.
[28] E. Verdin, F. Dequiedt, H. G. Kasler, *Trends Genet.* **2003**, *19*, 286 – 293.
[29] M. Göttlicher, S. Minucci, P. Zhu, O. H. Krämer, A. Schimpf, S. Giavara, J. P. Sleeman, F. Lo Coco, C. Nervi, P. G. Pelicci, T. Heinzel, *EMBO J.* **2001**, *20*, 6969 – 6978.
[30] T. Suzuki, T. Ando, K. Tsuchiya, N. Fukazawa, A. Saito, Y. Mariko, T. Yamashita, O. Nakanishi, *J. Med. Chem.* **1999**, *42*, 3001 – 3003.
[31] A. Saito, T. Yamashita, Y. Mariko, Y. Nosaka, K. Tsuchiya, T. Ando, T. Suzuki, T. Tsuruo, O. Nakanishi, *Proc. Natl. Acad. Sci. USA* **1999**, *96*, 4592 – 4597.
[32] J. C. Wong, R. Hong, S. L. Schreiber, *J. Am. Chem. Soc.* **2003**, *125*, 5586 – 5587.
[33] J.-H. Park, Y. Jung, T. Y. Kim, S. G. Kim, H.-S. Jong, J. W. Lee, D.-K. Kim, J.-S. Lee, N. K. Kim, T.-Y. Kim, Y.-J. Bang, *Clin. Cancer Res.* **2004**, *10*, 5271 – 5281.
[34] R. Fumurai, A. Matsuyama, N. Kobashi, K.-H. Lee, M. Nishiyama, H. Nakajima, A. Tanaka, Y. Komatsu, N. Nishino, M. Yoshida, S. Horinouchi, *Cancer Res.* **2002**, *62*, 4916 – 4921.
[35] R. Fumurai, Y. Komatsu, N. Nishino, S. Khochbin, M. Yoshida, S. Horinouchi, *Proc. Natl. Acad. Sci. USA* **2001**, *98*, 87 – 92.
[36] A. R. Guardiola, T.-P. Yao, *J. Biol. Chem.* **2002**, *277*, 3350 – 3356.
[37] S. M. Sternson, J. C. Wong, C. M. Grozinger, S. L. Schreiber, *Org. Lett.* **2001**, *3*, 4239 – 4242.
[38] S. J. Haggarty, K. M. Koeller, J. C. Wong, R. A. Butcher, S. L. Schreiber, *Chem. Biol.* **2003**, *10*, 383 – 396.
[39] S. J. Haggarty, K. M. Koeller, J. C. Wong, C. M. Grozinger, S. L. Schreiber, *Proc. Natl. Acad. Sci. USA* **2003**, *100*, 4389 – 4394.
[40] A. Mai, S. Massa, R. Pezzi, D. Rotili, P. Loidl, G. Brosch, *J. Med. Chem.* **2003**, *46*, 4826 – 4829.
[41] S. Massa, A. Mai, G. Sbardella, M. Esposito, R. Ragno, P. Loidl, G. Brosch, *J. Med. Chem.* **2001**, *44*, 2069 – 2072.
[42] A. Mai, S. Massa, R. Ragno, M. Esposito, G. Sbardella, G. Nocca, R. Scatena, F. Jesacher, P. Loidl, G. Brosch, *J. Med. Chem.* **2002**, *45*, 1778 – 1784.
[43] A. Mai, S. Massa, R. Ragno, I. Cerbara, F. Jesacher, P. Loidl, G. Brosch, *J. Med. Chem.* **2003**, *46*, 512 – 524.
[44] A. Mai, S. Massa, I. Cerbara, S. Valente, R. Ragno, P. Bottoni, R. Scatena, P. Loidl, G. Brosch, *J. Med. Chem.* **2004**, *47*, 1098 – 1109.
[45] R. Ragno, A. Mai, S. Massa, I. Cerbara, S. Valente, P. Bottoni, R. Scatena, F. Jesacher, P. Loidl, G. Broschl, *J. Med. Chem.* **2004**, *47*, 1351 – 1359.
[46] D. Kölle, G. Brosch, T. Lechner, A. Pipal, W. Helliger, J. Taplick, P. Loidl, *Biochemistry* **1999**, *38*, 6769 – 6773.
[47] T. Lechner, A. Lusser, A. Pipal, G. Brosch, A. Loidl, M. Goralik-Schramel, R. Sendra, S. Wegener, J. D. Walton, P. Loidl, *Biochemistry* **2000**, *39*, 1683 – 1692.
[48] G. Brosch, M. Goralik-Schramel, P. Loidl, *FEBS Lett.* **1996**, *393*, 287 – 291.
[49] G. Brosch, E. Georgieva, G. Lopez-Rodas, H. Lindner, P. Loidl, *J. Biol. Chem.* **1992**, *267*, 20561 – 20564.
[50] W. Pendergast, J. V. Johnson, S. H. Dickerson, I. K. Dev, D. S. Duch, R. Ferone, W. R. Hall, J. Humphreys, J. M. Kelly, D. C. Wilson, *J. Med. Chem.* **1993**, *36*, 2279 – 2291.
[51] Y. Tamura, *J. Med. Chem.* **1981**, *24*, 43 – 47.
[52] S. Munavalli, G. A. Bhat, C. Viel, *Bull. Soc. Chim. Fr.* **1966**, 3311 – 3318.
[53] J. V. Sinisterra, Z. Mouloungui, M. Delmas, A. Gaset, *Synthesis* **1985**, 1097 – 1100.
[54] K. Mori, K. Koseki, *Tetrahedron* **1988**, *44*, 6013 – 6020.
[55] HD2 activity was extensively purified by anion-exchange chromatography (Q-Sepharose), affinity chromatography (Heparin–Sepharose, Histone–Agarose), and size-exclusion chromatography (Superdex S200) as described in references [56–][58]
[56] T. Lechner, A. Lusser, G. Brosch, A. Eberharter, M. Goralik-Schramel, P. Loidl, *Biochim. Biophys. Acta* **1996**, *1296*, 181 – 188.
[57] G. Brosch, A. Lusser, M. Goralik-Schramel, P. Loidl, *Biochemistry* **1996**, *35*, 15907 – 15914.
[58] D. Kölle, G. Brosch, T. Lechner, A. Lusser, P. Loidl, *Methods* **1998**, *15*, 323 – 331.
[59] J. Kruh, *Mol. Cell. Biochem.* **1982**, *42*, 65 – 82.
[60] C. J. Phiel, F. Zhang, E. Y. Huang, M. G. Guenther, M. A. Lazar, P. S. Klein, *J. Biol. Chem.* **2001**, *276*, 36734 – 36741.
[61] M. Yoshida, M. Kijima, M. Akita, T. Beppu, *J. Biol. Chem.* **1990**, *265*, 17174 – 17179.
[62] V. M. Richon, S. Emiliani, E. Verdin, Y. Webb, R. Breslow, R. A. Rifkind, P. A. Marks, *Proc. Natl. Acad. Sci. USA* **1998**, *95*, 3003 – 3007.
[63] M. Kijima, M. Yoshida, K. Suguta, S. Horinouchi, T. Beppu, *J. Biol. Chem.* **1993**, *268*, 22429 – 22435.
[64] G. Brosch, R. Ransom, T. Lechner, J. Walton, P. Loidl, *Plant Cell* **1995**, *33*, 1941 – 1950.
[65] O. Lund, M. Nielsen, C. Lundegaard, P. Worning, Abstract, CASP5 Conference A102, **2002**. http://www.cbs.dtu.dk/services/CPHmodels/.
[66] A. Pipal, M. Goralik-Schramel, A. Lusser, C. Lanzanova, B. Sarg, A. Loidl, H. Lindner, V. Rossi, P. Loidl, *Plant Cell* **2003**, *15*, 1904 – 1917.
[67] J. R. Somoza, R. J. Skene, B. A. Katz, C. Mol, J. D. Ho, A. J. Jennings, C. Luong, A. Arvai, J. J. Buggy, E. Chi, J. Tang, B. C. Sang, E. Verner, R. Wynands, E. M. Leahy, D. R. Dougan, G. Snell, M. Navre, M. W. Knuth, R. V. Swanson, D. E. McRee, L. W. Tari, *Structure* **2004**, *12*, 1325 – 1334.
[68] D. A. Pearlman, D. A. Case, J. W. Caldwell, W. R. Ross, T. E. Cheatham III, S. DeBolt, D. Ferguson, G. Seibel, P. Kollman, *Comput. Phys. Commun.* **1995**, *91*, 1 – 41.
[69] J. W. Ponder, D. A. Case, *Adv. Protein Chem.* **2003**, *56*, 27 – 85.
[70] G. M. Morris, D. S. Goodsell, R. S. Halliday, R. Huey, W. E. Hart, R. K. Belew, A. J. Olson, *J. Comput. Chem.* **1998**, *19*, 1639 – 1662.
[71] D.-F. Wang, O. Wiest, P. Helquist, H.-Y. Lan-Hargest, N. L. Wiech, *J. Med. Chem.* **2004**, *47*, 3409 – 3417.
[72] A. Mai, M. Esposito, G. Sbardella, S. Massa, *Org. Prep. Proced. Int.* **2001**, *33*, 391 – 394.

[73] R. Sendra, I. Rodrigo, M. L. Salvador, L. Franco, *Plant Mol. Biol.* **1988**, *11*, 857 – 866.
[74] J. Wang, R. M. Wolf, J. W. Caldwell, P. A. Kollman, D. A. Case, *J. Comput. Chem.* **2004**, *25*, 1157 – 1174.
[75] A. W. Schuettelkopf, D. M. F. van Aalten, *Acta Crystallogr. Sect. D* **2004**, *60*, 1355 – 1363.
[76] P. De Baetselier, E. Scrham, *Methods Enzymol.* **1986**, *133*, 507 – 530.

Received: July 26, 2005
Revised: October 3, 2006
Published online on December 29, 2005

